IMPROVING THE LUMINESCENCE OF DOWN-SHIFTING MATERIALS FOR SOLAR CELLS BY CO-DOPING SILICA NANOPARTICLES WITH ORGANIC LANTHANIDES COMPLEXES

L. Bellotto[1], E. Moretti[1], M. Basile[1], C. Malba[1], F. Enrichi[2], S. Polizzi[1]

[1]Dipartimento di Scienze Molecolari e Nanosistemi, Università Ca' Foscari Venezia, Via Torino 155/b, 30172 Venezia-Mestre, Italy
[2]CIVEN, Coordinamento Interuniversitario Veneto per le Nanotecnologie, Via delle Industrie 5, 30175 Marghera (Venezia), Italy

ABSTRACT: $Eu(dbm)_3Phen$ and $Tb(dbm)_3Phen$ complexes have been impregnated in ordered mesoporous silica nanoparticles, with an average size of 50-70 nm and a pore diameter centered at 2.8 nm, with the aim of increasing the luminescence for their application as down-shifters for multicrystalline silicon solar cells. The morphological, structural, textural and luminescent properties of the synthesized samples were characterized by N_2 physisorption, X-ray diffraction (XRD), transmission electron microscopy (TEM), UV-visible spectroscopy and photoluminescence (PL and PLE) measurements.

Keywords: Nanoparticles, Down-shifting, Light harvesting, Photoluminescence

1 INTRODUCTION

Harnessing those regions of the solar spectrum which are only weakly, or not at all, converted into electricity by multicrystalline silicon solar cells is highly desirable, in order to increase efficiency and reach grid-parity. Down-shifters which convert UV radiation into visible or near infra-red light may serve this goal [1]; these materials need to efficiently absorb a broad spectral range between 300 nm and 450 nm and re-emit with a large Stokes shift in the region where the solar cells show a significantly better response. Lanthanide ions have sharp emission profiles with high internal efficiency, but their absorption is very small and it takes place only on very specific wavelengths; this may be appropriate for applications where excitation can be made by lasers, but not for solar spectrum conversion. However, if the lanthanide ion is conjugated with suitable organic ligands having an electronic structure which matches that of the lanthanide, the desired optical properties for this application may be obtained since the ligand act as an antenna capable to absorb efficiently a broad spectral region (typically in the UV) and to transfer energy to the rare earth ion, which emits in the visible. At the same time, in order to obtain a good quantum yield, the emitted radiation has not to be quenched by the chemical environment or the matrix in which the ions are included and/or by concentration quenching. Furthermore, the organic ligand may suffer from UV degradation or thermal instability.

In order to address such problems two synergic approaches have been tested in this paper. The first is that of hosting the complex molecules within the pores of properly synthesized mesoporous silica nanoparticles. The pores were chosen of suitable size in order to "dilute" the emitting ions, thus avoiding concentration quenching and at the same time protecting them from the environment. Such an approach has shown to improve luminescence in similar cases [2-5]. Since the final goal is to obtain a layer transparent to visible light, the mesoporous silica must be in the form of nanoparticles to avoid light scattering; such nanoparticles can be then dispersed in the cell encapsulating layer.

The second approach is that of co-doping with two different lanthanide complexes, where not only the antenna but also the second lanthanide ion can act as sensitizer for the first ion. To this purpose, the Tb^{3+}/Eu^{3+} pair is well known, where Tb ions can efficiently transfer energy to Eu ions increasing their emission in the red spectral region. In this situation UV light is absorbed by the ligand and then transferred to Eu ions either directly or indirectly mediated by Tb. Optimizing the ratio between Tb- and Eu- complexes within the pores of silica nanoparticles, it is possible to avoid concentration quenching [6] and obtain high red emission intensity.

2 EXPERIMENTAL

2.1 Materials

The two lanthanide complexes $Ln(dbm)_3Phen$ (with Ln=Eu, Tb) were synthesized according to the procedure reported by McGhee *et al.* [7].

Mesoporous silica nanoparticles (MSN) were synthesized according to the following procedure reported by Qiao *et al.* [8]. In a 500 mL round bottomed flask filled with 128 mL of deionized water; 22.8 mL ethanol, 5.73 g CTABr, 17.2 mL water, 1.25 mL 28% ammonia solution were added. The solution was stirred at 60 °C for 30 min, and 14.6 mL of TEOS were added dropwise keeping the mixture under continuous stirring for two more hours. The white solid precipitated was recovered by centrifugation (4 times 20 min at 9000 rpm) and subsequent sonication (30 min), by washing once with deionized water and three times with ethanol. The resulting solid was dried under reduced pressure and calcined at 600 °C for 6 h.

Doping of the silica nanoparticles with the Ln^{3+} complexes was obtained by wet impregnation. In a general procedure, $Ln(dbm)_3Phen$ (0 to x mg) was dissolved into CH_2Cl_2 (5 mL) and added to MSN (100 mg). The solution was stirred until complete evaporation of solvent and its residuals were removed under reduced pressure. The resulting solid was washed twice with the same solvent.

A series of samples with increasing amount of Eu-complex were prepared and labeled as Eu_x (x=0.2, 0.5, 2, 5, 10, 30, 40, 100), where x is the complex amount in mg per 100 mg of silica (corresponding to 0.2, 0.5, 2, 4.8, 9.1, 23.1, 28.6, 50 wt.% of $Eu(dbm)_3Phen$ calculated with respect to the overall weight of the sample respectively).

A further series of samples were prepared with different amounts of the two complexes: four series were obtained by keeping constant the amount of Eu-complex at x=0.2, 2, 5 and 10 mg, respectively and varying the Tb-complex amount 1, 2, 5, 20 times.

Samples were then labeled as Eu_xTb_y, where x and y represent the complexes amount in mg per 100 mg of silica. The nominal wt% of each complex was calculated with respect to the overall weight of the sample.

2.2 Characterization methods

Nitrogen adsorption-desorption measurements were performed at liquid nitrogen temperature (-196 °C) with an ASAP 2010 apparatus of Micrometrics. The analysis procedure is fully automated and operates with the static volumetric technique. Before measurement, the sample was outgassed first at 110 °C for 12 h at 5 10^{-3} Torr and then at room temperature for 2 h at 0.75 10^{-6} Torr. The N_2 isotherms were used to determine the specific surface areas through the BET equation and the specific pore volume calculated at p/p_0=0.98. The pore size distribution was calculated following the BJH method.

X-ray measurements have been carried out using a Philips X'Pert goniometer with Bragg-Brentano geometry, connected to a highly stabilized generator. A focusing graphite monochromator and a proportional counter with a pulse-height discrimination were employed (steps of 0.05° 2θ), with collection times of 10 s/step.

TEM images were taken at 300 kV with a JEOL 3010, equipped with a Gatan multi-scan CCD camera and an Oxford EDS microanalysis detector. TEM specimens were prepared by ultrasonically dispersing the powder samples in ethanol and depositing one drop of the suspension on a holey carbon film supported by a copper grid.

Absorption measurements were taken with a Agilent diode array spectrometer 8453.

Photoluminescence excitation, emission and time-resolved measurements were carried out using a Horiba-Jobin Yvon Fluorolog 3-21 spectrofluorimeter. A Xenon arc lamp was used as a continuous-spectrum source selecting the excitation wavelength by a double Czerny-Turner monochromator. The detection system was constituted by an iR300 single grating monochromator coupled to a R928 photomultiplier tube operating at 950 V. The excitation spectra were recorded in the 250-450 nm range with 1 nm bandpass resolution, dividing the PMT signal by intensity of the lamp, measured by using a calibrated photodetector. On the other hand, the emission spectra were recorded in the 550-750 nm range with 1 nm band-pass resolution and corrected for the response of the instrument.

Time-resolved analysis were performed in multi-channel scaling modality (MCS) by using a tunable Nd:YAG laser system as excitation source (wavelength selection from 210 to 2300 nm, 10 Hz repetition rate, 6 ns pulse duration). The decay profiles were fitted with least squares method, by using one or more exponential equations. Il all cases, χ^2 values near to 1 confirmed the high quality of the fitting.

3 RESULTS AND DISCUSSION

3.1 The Ln^{3+} complexes

Fig.1 shows the molecular sketches of the two Ln^{3+} complexes used in this paper. They are formed by one phenantroline and three dibenzoylmethane ligands connected by dative bonds to the lanthanoid ion, Eu^{3+} or Tb^{3+}, respectively.

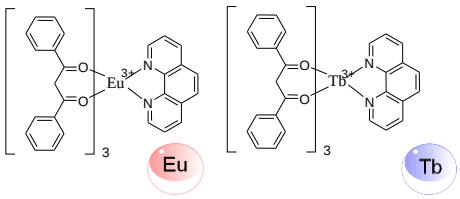

Figure 1: Molecular sketch of the used chromophores.

Fig. 2 shows absorption, excitation and emission spectra of the $Eu(dbm)_3Phen$ complex in solution. Absorption takes place on two bands: one, centred at 270 nm, is attributed to the absorption by the phenantroline ligand [6], and is of no interest for terrestrial solar applications; on the contrary, the second band, centred in the near UV region (320-400 nm, λ_{max} = 376 nm) and attributed to the dbm ligands [6], is of great interest since it harvests part of the AM1.5 solar spectrum which is not harnessed by Si-based solar cells.

The emission spectrum contains the red $^5D_0$-^7F_J (J=0, 1, 2, 3, 4) transition lines of the Eu^{3+} ion, with the most prominent hypersensitive transition $^5D_0$ - $^7F_2$ (612 nm). The excitation spectrum taken at 612 nm overlaps fairly well with the absorption spectrum, indicating that the energy transfer from the ligands to the Eu^{3+} ions takes place efficiently. In particular, the down-conversion of the near UV light absorbed by the dbm ligands into the red emission of the Eu^{3+} would be ideal for the application to Si-based solar cells.

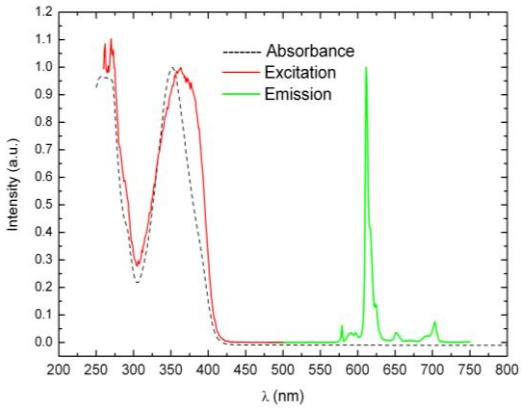

Figure 2: Absorption (dashed black), excitation (red) and emission (green) spectra of $Eu(dbm)_3Phen$ in CH_2Cl_2 solution (intensities have been suitably scaled)

3.2 Silica Mesoporous Nanoparticles (MSN)

In order to preserve such an ideal behaviour when the complex is used introduced into a material avoiding concentration quenching, the complex has been included into mesoporous silica nanoparticles.

Fig 3 shows a typical TEM image of the synthesized silica nanoparticles. The MSN are roundish and have a diameter of about 50-70 nm.

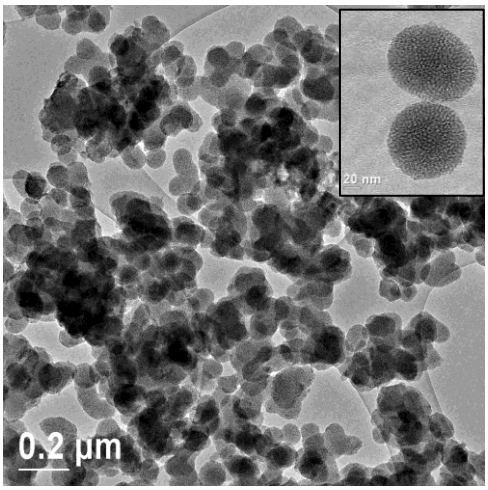

Figure 3: TEM images of the silica nanoparticles; the mesoporous structure is visible in the inset, which is taken at a higher magnification.

This size avoids scattering of the incoming light for wavelengths larger than 200 nm, allowing a high transparency for the spectral range harnessed by solar cells.

The ordered channel system can be clearly observed in the TEM micrographs by the pattern that appears when the image is slightly under-focused (see inset of Fig.3); the pattern suggests the presence of channels opened on the surface of the particle. The overall specific surface area, measured by BET equation, is approximately 1000 m^2/g with a total pore volume of 1.06 cm^3/g, and a narrow pore diameter distribution, centred at 2.8 nm which indicates the average size of the channel openings.

Comparing the pore diameter with the structural data of crystalline $Eu(dbm)_3phen$ [9], which indicates a triclinic unit cell containing four full molecules (P-1, with α = 103.844(6)°, β = 91.466(6)°, γ = 101.585(6)°, a = 1.6275(6) nm, b = 2.3504(9) nm and c =3.171(1) nm,) it can be argued that the pore openings are sufficiently large to let the complex molecules enter the channels and host at least one complex molecule.

By using the density value (1.446 g cm^{-3}) for a crystalline arrangement reported in the same paper [9] and the measured total pore volume, the maximum theoretical amount of complex which could be hosted within the MSNs has been estimated to be 140 wt.% of the silica matrix. This is of course an overestimated value, because the impregnation procedure will not allow to accommodate the complex molecules in a compact manner as in the crystalline state, completely filling the whole pore volume. However, it is a useful upper limit for the complex loading.

3.3 Eu-doped MSN

The silica samples impregnated with the Eu-complex were measured by XRPD and no crystalline peaks were detected. This could be taken as an indication of the dispersion of the complex on a molecular level, but the formation of an amorphous phase or crystals too small to be detected cannot be excluded.

TEM images of the impregnated materials do not show the presence of Eu-complex agglomerates outside of the silica particles until 23 wt.% ca. is reached. At this loading (sample Eu_{30}) amorphous agglomerates start to show up (see Fig.4) and become more frequent for higher loadings. EDX analysis confirms that such agglomerates are indeed of Eu-complex and, at the same time, it detects the presence of europium in the MSN, indicating that the Eu-complex has entered the pores of the impregnated MSN.

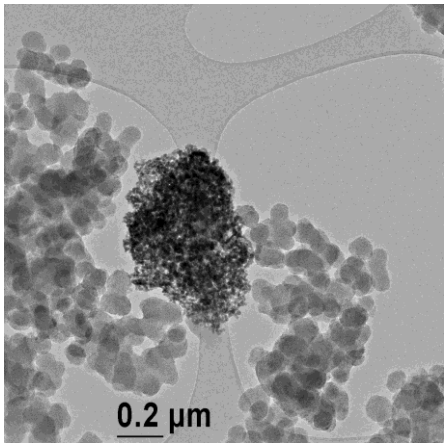

Figure 4: TEM images of samples Eu_{30} in an area where Eu-complex agglomerates outside of the nanoparticles are visible.

The shape of the emission spectrum does not change significantly when the Eu-complex is included in the MSN (not shown), and the intensity of the hypersensitive $^5D_0$-$^7F_2$ peak shows a linear increase with increasing loading up to about 25 wt.%, where it starts to bend towards an asymptotic behaviour. The limit value of the linear range corresponds to about 70 wt.% of the estimated maximum loading and it coincides with the load value from which external agglomerates have been observed by TEM. This suggests that concentration quenching starts to take place when the complex molecules are not confined within the pores.

However, looking at the excitation spectra (Fig.5, samples $Eu_{0.5}$ and Eu_{40} taken as an example), it is possible to observe that even for small amounts of Eu-complex the band in the near UV range is significantly different from the one of the complex in solution and it greatly differs from the absorption band, which, on the contrary, does not change its shape (not shown). The UV band becomes asymmetric and its maximum moves from 350 to about 400 nm, where absorption is low. This suggests a change in the electronic structure of the complex, which could be due to the evolution from that of a single molecule towards that of a solid state configuration, due to the vicinity of other molecules within the pores. Whatever the explanation be, this implies that energy transfer between the dbm ligand and the Eu^{3+} ion has lost in efficiency and that the transfer

takes place preferentially on the tail of the absorption band, i.e. most of the energy absorbed by the cromophore seems to be wasted. For larger amounts of Eu-complex the left side of the band is growing, progressively filling the region where absorption takes place. While this could represent an improvement in the down-conversion properties, it must be recalled that, for samples with higher loadings, complex aggregates have been found by TEM outside the pores and that the emission intensity has shown a decrease in efficiency, so that the change in the excitation spectrum could be actually related to molecules outside the pores, in aggregated and/or molecular form (not detectable by TEM).

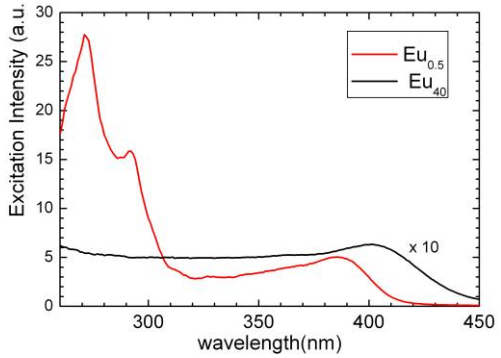

Figure 5: Excitation spectra of silica samples with different amount of Eu(dbm)$_3$Phen: $Eu_{0.5}$ and Eu_{40}.

Besides the increase of the left side of the band, a red shift of the maximum of excitation is observed from 386 nm to 401 nm (inset of Fig. 5). This part of the excitation could be due to molecules inside the pores whose electronic structure goes progressively towards a solid state configuration. In conclusion, the dispersion of very high amounts of cromophore molecules in a porous matrix does not seem to avoid clustering of Eu-complex molecules with possible concentration quenching.

3.4 Co-doped MSN

As stated above, co-doping is a further possible mean to keep Eu ions enough apart to avoid concentration quenching, besides possibly giving a further increase in the sensitizing effect to the Eu ions. To this aim a Tb-complex with the same ligands has been used: it absorbs in the same region but, due to energy levels proximity between triplet states of the ligands and $^5D_4$ level of the Tb ion, negligible luminescence is observed. The terbium complex should work as solar "accumulator" for the Eu complex: the solar energy is absorbed by the complex and transferred via Foster resonance energy transfer (FRET) to the Eu-complex augmenting the number of photons converted into visible region and keeping low the amount of Eu ions (Fig.6).

Considering that FRET depends upon the donor to acceptor distance with an inverse 6th power [10], the impregnation of both Eu- and Tb-complexes into the pores of mesoporous silica nanoparticles should keep the two complexes sufficiently close to one another, maintaining at the same time Eu-Eu ions distances sufficiently large.

Since the results on the Eu_x samples showed that complex aggregates form outside the pores for loadings higher than about 25 wt.%, the total loading of the lanthanide complexes in the co-doped samples was kept below that value.

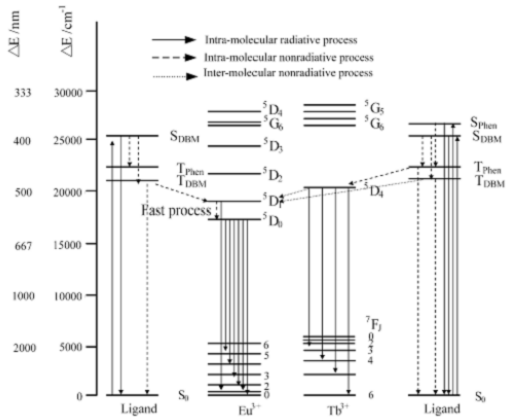

Figure 6: Scheme representing the energetic levels of Eu-Tb complexes and the relevant emission processes.

The emission profiles of all the co-doped samples (not shown) as well as lifetime measurements at 618 nm (not shown) do not show any significant difference from the singly-doped samples. This demonstrates that the Tb complex is able to fully transfer its energy to Eu^{3+} ions.

The energy transfer from Tb(dbm)$_3$Phen to Eu(dbm)$_3$Phen seems to take place since the emission intensity increases with increasing Tb loading at constant Eu amount (Fig.7). However, this happens only when the total complex amount is lower than about 10 mg/100 mg SiO_2. For the samples $Eu_{10}Tb_y$, the addition of the Tb-complex does not seem to have any effect.

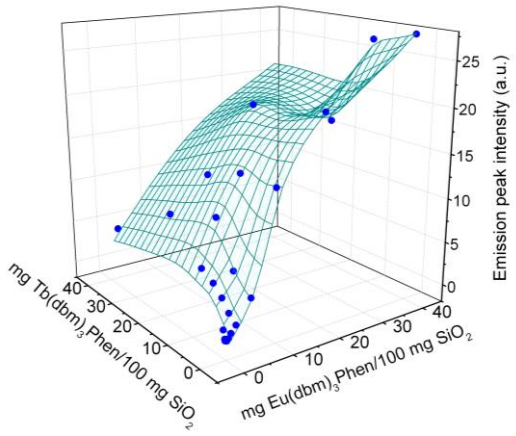

Figure 7: Emission intensity for increasing Tb-complex amounts at different Eu-complex loading (expressed as mg Ln(dbm)$_3$Phen/100 mg SiO_2).

The excitation spectra of the co-doped samples all show similar profiles (in Fig.8 sample $Eu_{0.2}Tb_4$ is reported as an example) and show a shift similar to the single-doped samples. The Tb-complex seems not to help in a better match of the excitation with absorption range, which would be desirable for a good luminescence yield. This can suggest that the electronic levels of the Eu-

complex are moving towards a solid-state structure also in the presence of Tb-complex molecules.

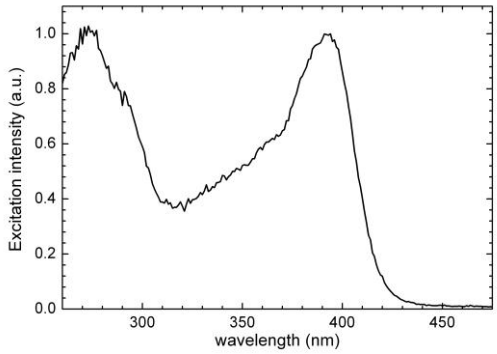

Figure 8: Excitation spectrum of the sample $Eu_{0.2}Tb_4$ (normalized to the peak intensity).

4 CONCLUSIONS

The inclusion of $Eu(dbm)_3Phen$ inside mesoporous silica nanoparticles, either alone or together with $Tb(dbm)_3Phen$, seems to have a positive effect on internal quantum efficiency, since the emission increases linearly up to high Eu-loadings, however it does not avoid a modification of the electronic structure of the complex which decreases the external quantum efficiency, since a large part of the absorbed UV energy is not transformed into red emission. Co-doping the material with $Tb(dbm)_3Phen$ enhances the emission only for low total amount of complex.

References

[1] E. Klampaftis, D. Ross, K.R. McIntosh, B.S. Richards, Sol. Energy Mat. Sol. Cells 93(8) (2009) 1182.
[2] X. Qinghong, L. Liansheng, L. Bin, Y. Jihong, X. Ruren, Micropor. Mesopor. Mater. 38(2-3) (2000) 351.
[3] Q. Xu, L. Li, X. Liu and R. Xu, Chem. Mater. 14 (2002) 549.
[4] Y. Li, B. Yan, Y. Li , J. Solid State Chem. 183 (2010) 871.
[5] D. Zhang, D. Tang, X. Wang, Z. Qiao, Y. Li. Y. Liu, Q. Huo, Dalton Trans. 40 (2011) 9313.
[6] Y. Luo, Q. Yan, S. Wu, W. Wu, Wenxuan and Q. Zhang, J. Photochem. Photobiol. A-Chem. 191(2-3) (2007) 91.
[7] M.D. McGehee, T. Bergstedt, C. Zhang, A.P. Saab, M.B. O'Regan, G.C. Bazan, V.I. Srdanov, A.J. Heeger, Advanced Materials, 11 (1999) 1349.
[8] Z.A. Qiao, L. Zhang, M. Guo, Y. Liu and Q. Huo, Chem Mater. 21 (2009) 3823.
[9] M.O. Ahmed, J.L. Liao, X. Chen, S.A. Chen, J.H. Kaldis, Acta Cryst. Section E, 59(1) (2003) 29.
[10] T. Forster, Ann. Phys. 2 (1948) 55.